






Constraining the Black Hole Initial Mass Function with LIGO/Virgo Observations

Rosalba Perna^{1,2} , Yi-Han Wang¹, Will M. Farr^{1,2} , Nathan Leigh^{1,3,4}, and Matteo Cantiello^{2,5} ¹ Department of Physics and Astronomy, Stony Brook University, Stony Brook, NY 11794, USA; rosalba.perna@stonybrook.edu² Center for Computational Astrophysics, Flatiron Institute, 162 5th Avenue, New York, NY 10010, USA³ Departamento de Astronomía, Facultad de Ciencias Físicas y Matemáticas, Universidad de Concepción, Concepción, Chile⁴ Department of Astrophysics, American Museum of Natural History, Central Park West and 79th Street, New York, NY 10024, USA⁵ Department of Astrophysical Sciences, Princeton University, Princeton, NJ 08544, USA

Received 2019 January 8; revised 2019 May 13; accepted 2019 May 21; published 2019 June 5

Abstract

Prior to the detection of black holes (BHs) via the gravitational waves (GWs) that they generate at merger, the presence of BHs was inferred in X-ray binaries, mostly via dynamical measurements, with masses in the range between ~ 5 and $20 M_{\odot}$. The Laser Interferometer Gravitational-Wave Observatory (LIGO) discovery of the first BHs via GWs was surprising in that the two BHs that merged had masses of $35.6_{-3.0}^{+4.8}$ and $30.6_{-4.4}^{+3.0} M_{\odot}$, which are both above the range inferred from X-ray binaries. With 20 BH detections from the first/second observing (O1/O2) runs, the distribution of masses remains generally higher than the X-ray inferred one, while the effective spins are generally lower. This suggests that, at least in part, the GW-detected population might be of dynamical origin rather than produced by the common evolution of field binaries. Here we perform high-resolution N -body simulations of a cluster of isolated BHs with a range of initial mass spectra and upper mass cutoffs, and study the resulting binary mass spectrum resulting from the dynamical interactions. Our clusters have properties that are similar to those of the massive remnants in an OB association ~ 10 Myr after formation. We perform a likelihood analysis for each of our dynamically formed binary population against the data from the O1 and O2 LIGO/Virgo runs. We find that an initial mass spectrum $M_{\text{BH}} \propto M^{-2.35}$ with an upper mass cutoff $M_{\text{max}} \sim 50 M_{\odot}$ is favored by the data, together with a slight preference for a merger rate that increases with redshift.

Key words: binaries: general – black hole physics – gravitational waves – methods: numerical

1. Introduction

The existence of black holes (BHs) is one of the primary predictions of the Theory of General Relativity. Prior to their direct discovery via the gravitational waves (GWs) that they generated in a merger event (Abbott et al. 2016b), their presence was inferred via dynamical mass measurements in X-ray binaries (see, e.g., Wiktorowicz et al. 2014 for a summary). The values of the inferred masses vary between ~ 4 and $5 M_{\odot}$ to about $20 M_{\odot}$, marking a clear separation with the inferred neutron star masses, for which the largest measurement to date is $1.96 M_{\odot}$ (Demorest et al. 2010).

The discovery of the first binary BH (BBH) merger via the GWs generated at the time of coalescence led to a mass measurement for the BH components of the merging binary: $35.6_{-3.0}^{+4.8}$ and $30.6_{-4.4}^{+3.0} M_{\odot}$. The large BH masses were both above the maximum value measured to date in X-ray binaries (Abbott et al. 2016a). The discovery triggered an intense debate in the literature on the formation pathway of this BH binary.

Broadly speaking, most formation avenues can be classified within one of two channels: isolated binary evolution, in which two massive stars evolve until their death while remaining gravitationally bound (e.g., Podsiadlowski et al. 2003; Dominik et al. 2013; Belczynski et al. 2016; Mandel & de Mink 2016; Marchant et al. 2016), or dynamical formation by gravitational capture in dense environments, where binaries are being formed from isolated BHs as a result of frequent dynamical interactions (e.g., Sigurdsson & Hernquist 1993; Portegies Zwart & McMillan 2000; O’Leary et al. 2006; Miller & Lauburg 2009; Mapelli et al. 2013; Leigh et al. 2014; Ziosi et al. 2014; Antonini et al. 2016, 2019; Rodriguez et al. 2016; Chatterjee et al. 2017; Banerjee 2018; Fragione & Kocsis 2018; Fragione et al. 2018; Generozov et al. 2018; Rodriguez &

Loeb 2018; Samsing 2018; Samsing & D’Orazio 2018; Di Carlo et al. 2019; Ye et al. 2019). The theoretically predicted rates are rather uncertain for both scenarios: the models explored by Belczynski et al. (2016) yield rates that vary between ~ 6 and $1000 \text{ Gpc}^{-3} \text{ yr}^{-1}$. More recent state-of-the-art estimates of the rates of dynamical formation in globular clusters yield a range of $4\text{--}18 \text{ Gpc}^{-3} \text{ yr}^{-1}$ (Rodriguez & Loeb 2018). Both of these rates are compatible with the current observationally determined value by the Laser Interferometer Gravitational-Wave Observatory (LIGO), of $9.7\text{--}101 \text{ Gpc}^{-3} \text{ yr}^{-1}$ (The LIGO Scientific Collaboration & the Virgo Collaboration 2018). In principle, both channels can contribute to the observed population, something that can be tested as many more mergers are going to be detected in the future.

To date, after the first two observing runs of LIGO/Virgo, there have been 10 BBH mergers reported (The LIGO Scientific Collaboration & the Virgo Collaboration 2018). While the smallest masses (four out of 20) fall within the upper range of the masses inferred for X-ray binaries, the other 16 are all larger, with the largest being $50.6_{-10.2}^{+16.6} M_{\odot}$. While the distributions are clearly not disjointed, there is a marked preference in GW-detected BHs for larger masses than in those found via X-ray binaries, raising the question of whether the two observed populations are dominated by the same progenitor population.

An independent piece of evidence that raises the same question is constituted by the measured spins⁶ (see, e.g., Farr et al. 2017; Roulet & Zaldarriaga 2019): generally high and aligned with the orbital angular momentum in the X-ray bursts

⁶ What GWs measure is the so-called effective spin, i.e., the mass-weighted projection of the spins onto the orbital angular momentum.

(especially the persistent ones), and typically low and isotropic in the GW-detected BHs. This trend is consistent with studies suggesting that, while isolated binaries preferentially yield BHs with spins aligned with the orbital angular momentum (i.e., Kalogera 2000), dynamically formed BHs have no preferred direction for alignment (i.e., Portegies Zwart & McMillan 2000).

In this Letter we investigate the possibility that the observed BH population is dominated by a dynamical formation channel complementary to the dynamical channel discussed in the context of globular clusters. More specifically, we generate small clusters of BHs with properties appropriate for the massive remnants of an OB association ~ 10 Myr after its formation, following the supernovae explosions of its massive constituents. Therefore, albeit dynamically formed, the binary population discussed here does not necessarily need to originate in globular clusters, but could also be associated with field stars. Using high-resolution N -body simulations of these clusters with a range of mass spectra, we explore the dependence of the BH binary mass distribution on the mass spectrum and upper mass cutoff of the individual BHs (Section 2). We perform a statistical comparison with the data from the first observing (O1) and second observing (O2) LIGO/Virgo runs to study the consistency between the data and the simulation results, and assess statistical preferences toward an initial BH mass spectrum (Section 3). We summarize and conclude in Section 4.

2. The BBH Mass Spectrum from Dynamical Interactions

Motivated by the considerations of Section 1, here we set to perform high-resolution N -body simulations of a cluster of BHs, with the goal of exploring the dependence of the mass spectrum and the orbital parameters of the dynamically formed binaries on the mass spectrum of the isolated BH population. We note that the mass spectrum of BH binaries produced as a result of dynamical interactions in clusters has a long history in the literature, predating the era of GWs. A preferential tendency for dynamically formed binaries to have heavier masses has been noted in a number of works (O’Leary et al. 2006; Miller & Lauburg 2009; Ryu et al. 2016; Rodriguez et al. 2018; Di Carlo et al. 2019). While not including the effects of the cluster potential, our fewbody simulations allow us to accurately follow binary formation (because in dense environments this is dominated by three-body scatterings), as well as perform a large number of Monte Carlo realizations.

We consider a cluster of 20 BHs, with an initial binary fraction equal to zero, in order to purely explore the binary properties due to dynamical formation. Their positions in the cluster are initially distributed randomly in a sphere of radius 0.1 pc. Astrophysically, this configuration can be thought of as representing the remnants of an OB association (typically comprising ~ 10 – 100 stars), still confined within the dense core of a molecular cloud⁷ (e.g., Zhou et al. 1994). From a numerical point of view, we note that the particular number of 20 was chosen as a “sweet spot”: large enough for obtaining a reasonably well-sampled binary mass distribution, but small enough to enable the running of a large number of realizations with high numerical accuracy. However, we ran several

additional simulations with different numbers of BHs in order to verify that the shape of the binary distribution remains statistically the same as the number of BHs is varied. Similarly, we chose the size of the initial spatial domain after verifying that it was large enough that the results for the binary mass distributions were converged as the region size was varied.

The BHs were assigned a mean speed of 5 km s^{-1} , as typical of the velocity dispersions observed in low-mass star clusters (e.g., Harris 1996). We follow their evolution using our code *SpaceHub*⁸ (see Wang et al. 2019 for details), which employs the *ARCHAIN* algorithm (Mikkola & Merritt 2008) to accurately trace the motion of tight binaries with arbitrarily large mass ratios and eccentricities, and a chain structure to reduce the round-off errors from close encounters. Binaries are detected in the simulations when the following conditions are verified: (a) the BH masses m_1 and m_2 are gravitationally bound to one another; (b) the system ($m_1 + m_2$) is gravitationally unbound in the potential of the remaining BHs; (c) the binary has traveled a large enough distance from the original BH cluster. We chose the distance to be 20 times the size of the original cluster, after verifying that the simulation results are converged for that value. The initial BH masses are drawn from a distribution with $M_{\min} = 5M_{\odot}$ and M_{\max} varying within the range 40 – $50 M_{\odot}$ in steps of $5 M_{\odot}$. The mass spectrum of BH remnants, in addition to depending on the evolutionary model, is also strongly dependent on metallicity, varying from an almost flat distribution at solar metallicities to an almost linear dependence on the main sequence mass at low metallicities and for high-mass progenitor stars (e.g., Spera et al. 2015). Therefore, we explored a variety of mass spectra, ranging from a flat distribution to a power-law $M^{-\alpha}$ with index $\alpha = 4$ in steps of 0.5. Additionally, we also investigated the particular case of $M^{-2.35}$, corresponding to a BH mass spectrum reflective of the initial mass function of the massive progenitor stars (Salpeter 1955).

We show some representative results in Figure 1 ($\alpha = 1$), Figure 2 ($\alpha = 2$), and Figure 3 ($\alpha = 3$), all with $M_{\max} = 50 M_{\odot}$. In the left panels we show the mass ratio q , while the right panels show the merger time τ_{GW} calculated according to Peters’ formulae (Peters 1964), both versus the total mass of the binaries. The flatter mass spectrum ($\alpha = 1$) yields a large fraction of binaries with total mass ~ 40 – $65 M_{\odot}$. Interestingly, not only is there an exceedingly large number of very massive binaries formed, but they are also the ones that are more tightly bound, hence resulting in shorter merger times due to GW emission (note a similar result found by Ryu et al. 2016 in the context of the formation of the first X-ray binaries). The most massive binaries also tend to have higher mass ratios. Note that the kink at $\sim 55 M_{\odot}$ corresponds to the mass of the binary formed by the most- and the least-massive BHs, which results in the mass distribution undergoing a change of slope as it passes through that point.

As the mass spectrum steepens to M^{-2} , the distribution becomes more apparently dominated by lower-mass binaries, but a tail in the high-mass range still remains. For $\alpha = 3$, the binary mass distribution becomes clearly peaked toward low masses, and the high-mass tail of the distribution becomes vanishingly small. The fraction of BHs that end up as ejected binaries is also dependent on the mass spectrum. In particular, we found this fraction to be 0.11% for $\alpha = 1\%$, 0.09% for

⁷ Dynamically, however, this population bears resemblance with a core-collapsed cluster (see e.g., Sigurdsson & Hernquist 1993; Rodriguez et al. 2016).

⁸ <https://github.com/YihanWangAstro/Template-SpaceX>

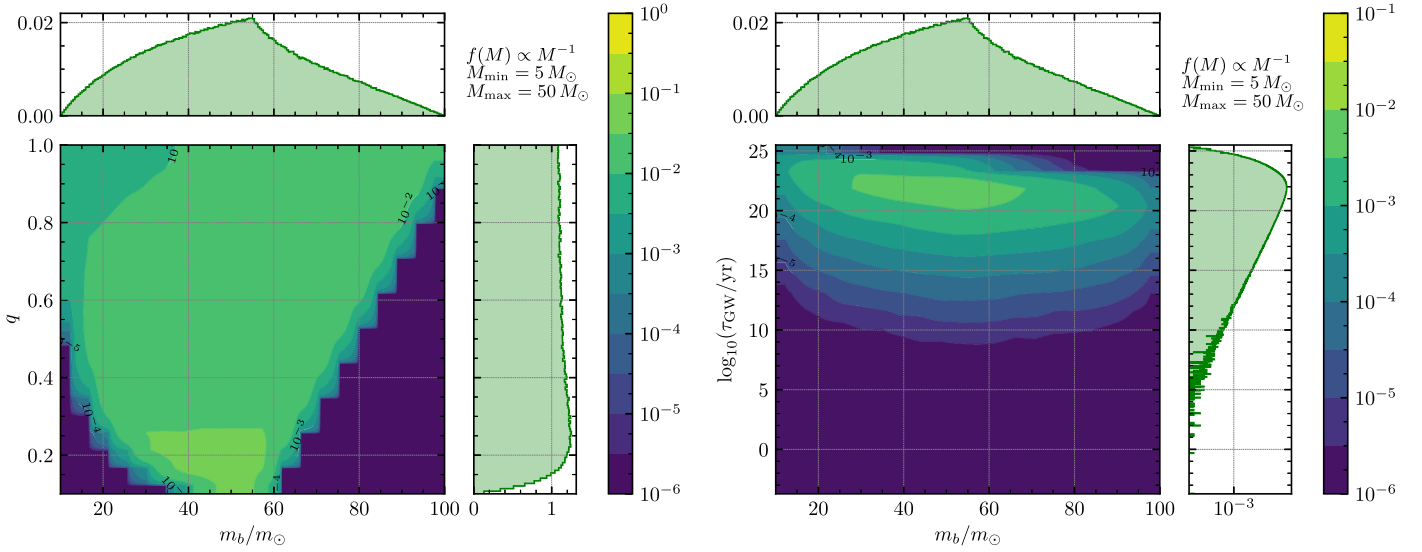


Figure 1. Left panel: the distribution of mass ratios and total binary masses of dynamically formed binaries from a cluster of BHs with a mass spectrum $\propto M^{-1}$ between 5 and $50 M_{\odot}$. Right panel: the corresponding merger times as a function of the total binary masses. In both panels, the top and the right plots display the collapsed 2D distributions onto the corresponding axis.

$\alpha = 2\%$, and 0.065% for $\alpha = 3$. Correspondingly, the relative fraction of those binaries that merge within the Hubble time is 0.092% , 0.069% , and 0.048% for $\alpha = 1, 2, 3$, respectively.

Of particular relevance for the LIGO/Virgo results is the fact that the more massive binaries tend to be the more tightly bound; the heaviest objects are in fact the ones with the largest cross-sections for encounters, hence they undergo the most scatterings and end up as the hardest binaries. This tendency is especially pronounced for shallower BH mass spectra, when the number of massive BHs is not much smaller than the number of lighter BHs. For very steep slopes of the mass spectrum, the interaction probability becomes dominated by the number of small BHs, which hence have much higher chances of interacting and thus forming tight binaries.

3. Statistical Comparison with the LIGO/Virgo Data from the O1/O2 Runs

We now wish to compare the models described in the previous section to the 10 binary BH mergers observed by LIGO and Virgo in GWTC-1 (The LIGO Scientific Collaboration & the Virgo Collaboration 2018).⁹ The analysis is very similar to Farr et al. (2017): here we have a collection of zero-parameter models that predict the mass distribution of merging BHs. Unlike in Farr et al. (2017), the detectability of mergers is a strong function of mass, so we must account for selection effects; see Mandel et al. (2019) and references therein.

We are comparing to a data set, \mathbf{d} , consisting of a catalog of detections, $i = 1, \dots, N_{\text{det}} = 10$. The Bayesian posterior probability of a particular mass model, M , is given by

$$p(M|\mathbf{d}) \propto p(\mathbf{d}|M)p(M). \quad (1)$$

$p(\mathbf{d}|M)$ is sometimes known as the ‘‘Bayes factor;’’ it is the likelihood of model M given the observed data. $p(M)$ is the prior probability of model M , which we are free to assign based on our experience and intuition; we describe our model priors below as we discuss Figure 4.

We assume that the noise realization in the LIGO and Virgo detectors is statistically independent for each event, so that

$$p(\mathbf{d}|M) = \prod_{i=1}^{N_{\text{det}}} p(d_i|M). \quad (2)$$

Each model makes predictions about the masses of the merging binaries. In principle each model also makes predictions about the redshift distribution of merging binaries, but we leave study of this prediction to future work. Instead, we select only the mergers whose time to merger is $t_{\text{GW}} < 10^{10}$ yr and, following Fishbach et al. (2018), impose a parameterized redshift distribution of events corresponding to a volumetric merger rate in the comoving frame of

$$\frac{dN}{dVdt} \propto (1+z)^{\lambda}. \quad (3)$$

Setting $\lambda = 3$ gives a merger rate that approximately tracks the star formation rate; setting $\lambda = 0$ gives a merger rate that is constant in the comoving frame (Fishbach et al. 2018). The likelihood of the data depends on the masses and redshifts of the merging systems, which are subject to selection effects, so we have (Farr et al. 2017; Mandel et al. 2019)

$$p(d_i|M) = \frac{\int dm_1 dm_2 dz p(d_i|m_1, m_2, z)p(m_1, m_2, z|M)}{\int dm_1 dm_2 dz P_{\text{det}}(m_1, m_2, z)p(m_1, m_2, z|M)}. \quad (4)$$

Here the numerator is the likelihood of the LIGO data given the masses and redshifts predicted by the model M , and the denominator is the correction for the selection function and gives the average detectability for the model population.

The denominator is independent of the data, d_i , and common to all events. We use a Monte Carlo estimate of the integral (Farr 2019) obtained by generating synthetic merger events and detecting them using an analytic estimate of the LIGO/Virgo O1+O2 sensitivity (Abbott et al. 2016c).

⁹ Our analysis can be found at <https://github.com/farr/ClusterBHGW>.

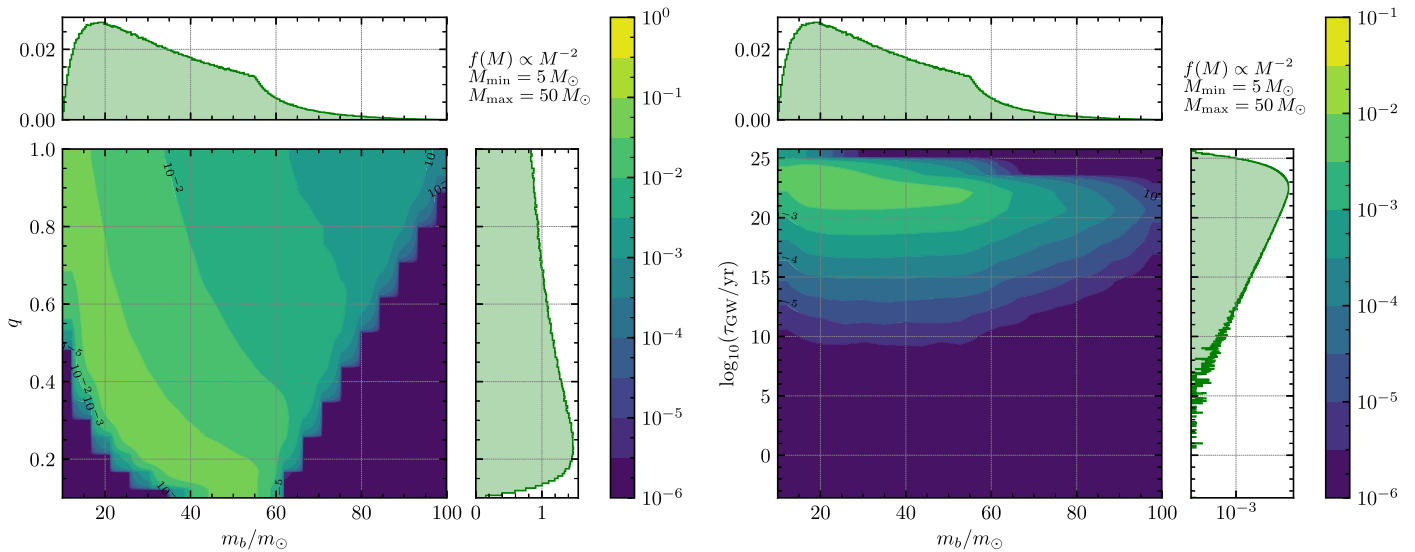


Figure 2. Same as in Figure 1 but for a power-law mass spectrum of index -2 for the interacting isolated BHs.

The numerator can also be computed via Monte Carlo using parameter estimation samples from The LIGO Scientific Collaboration & the Virgo Collaboration (2018). Those are drawn from a posterior density that incorporates the likelihood and a prior, $p_{\text{PE}}(m_1, m_2, z)$ (where PE stands for parameter estimation)

$$m_1, m_2, z \sim p(d_i|m_1, m_2, z)p_{\text{PE}}(m_1, m_2, z), \quad (5)$$

so the likelihood integral that we need can be computed via

$$\int dm_1 dm_2 dz p(d_i|m_1, m_2, z)p(m_1, m_2, z|M) \propto \left\langle \frac{p(m_1, m_2, z|M)}{p_{\text{PE}}(m_1, m_2, z)} \right\rangle, \quad (6)$$

where the final average is taken over the PE samples. We use a Gaussian kernel density estimator in a 2D, unconstrained parameter space $(x, y) = (\log m_1, \log m_2 - \log(m_1 - m_2))$ to smooth the distribution over masses predicted by each model when computing the model likelihood.

We begin our analysis by considering, for each of the models described in Section 3, a population drawn from a redshift distribution varying from constant ($\lambda = 0$), to a rapidly evolving one ($\lambda = 6$). We impose uniform prior density in models in α and λ . The 2D posterior on models in α - λ space is displayed in Figure 4, together with the 1D projections on the λ and α axis, for the case with $M_{\text{max}} = 50 M_{\odot}$, which appears to provide the best match.

The analysis shows that there is a slight preference for an evolving redshift distribution, though the trend is only marginal. This is consistent with the results on redshift evolution from The LIGO Scientific Collaboration et al (2018). Marginalizing over λ , the preferred spectral index is found to be $\alpha = 2.35$. A rough 1σ (68% credible) interval for α is $\alpha = 2.35^{+0.55}_{-0.36}$.

In Figure 5 we compare our models' predictions for the distribution of the observed total mass of 10 merging binaries for various values of M_{max} , fixing $\lambda = 3$ (i.e., a merger rate that tracks the star formation rate), and $\alpha = 2.35$. The predictions incorporate both the GW selection function and also observational uncertainties. No model fully reproduces the distribution

of observed total masses, though the observations lie within the 1σ band of the $M_{\text{max}} = 50 M_{\odot}$, $\alpha = 2.35$ model. We remark that our models are minimally parameterized, being dependent only on the two parameters α and M_{max} ; the shape of the binary mass distribution is then determined by dynamics alone, and hence its resemblance to the observed distribution for some astrophysically interesting sets of parameters ($\alpha = 2.35$ and $M_{\text{max}} = 50 M_{\odot}$) is especially intriguing.

4. Summary

The discovery of BHs via the GWs emitted when they merge in a binary has confirmed one of the milestone predictions of the Theory of General Relativity, while at the same time opening a new window into our exploration of the universe. As often happens with new observations, this new window has also raised some questions. In the case of the 20 BHs discovered by the LIGO/Virgo collaboration via their mergers in binaries during the O1/O2 runs, their mass spectrum has been somewhat surprising, being shifted toward larger masses with respect to the BHs whose masses had previously been measured dynamically in X-ray binaries. The measured spins, on the other hand, have been found to be mostly consistent with low and isotropic ones, unlike the generally high ones measured in X-ray binaries.

In this Letter we have investigated the possibility that X-ray and GW-detected BHs are dominated by different formation channels: isolated binary evolution for the former, and (primarily) dynamical formation for the latter. Via high-resolution N -body simulations of a mini-cluster of initially isolated BHs (which can be thought of as the remnants of an OB association), we have shown a tendency for binary BH formation among the heaviest objects in the cluster (see also O'Leary et al. 2006; Rodriguez & Loeb 2018; Di Carlo et al. 2019 for similar trends in globular clusters). The heaviest BH binaries tend to also be the ones that are more tightly bound, hence resulting in shorter merger times, which enhances the probability of being detected via GWs.

While weighed toward larger masses, the precise shape of the mass distribution of the dynamically formed binary BHs is also reflective of the particular initial BH mass function. We investigated this distribution for a variety of BH mass spectra,

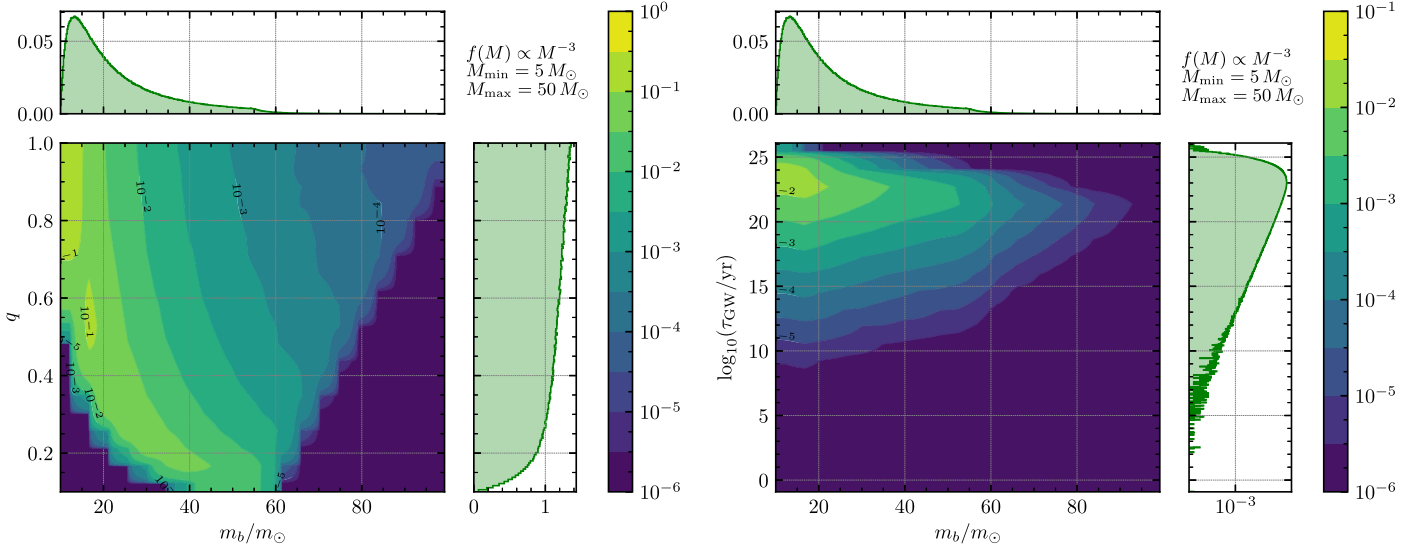


Figure 3. Same as in Figure 1 but for a power-law mass spectrum of index -3 for the interacting isolated BHs.

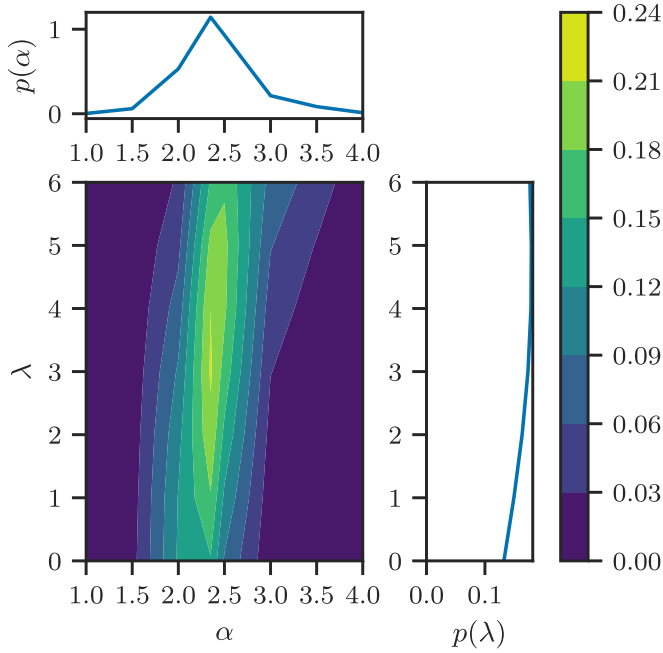


Figure 4. 2D posterior on α (slope of the BH mass function) and λ (slope of the merger rate vs. redshift) inferred from the 10 LIGO/Virgo BBH detections discussed in Section 3 and the 1D marginal posteriors for α and λ . We impose a flat prior density in α and λ . The observations weakly favor a merger rate that increases rapidly with redshift ($\lambda \simeq 3$ corresponds to a merger rate that tracks the star formation rate Madau & Dickinson 2014; Fishbach et al. 2018). The posterior is maximized (in both 1 and 2D) at $\alpha = 2.35$, with a 1σ (68% credible) interval of $\alpha = 2.35^{+0.55}_{-0.36}$.

from a flat distribution to a power law with an index of -4 , and extracted the sub-population of dynamically formed binaries that merge within a Hubble time. We therefore performed a Bayesian statistical analysis to compare the likelihood of each of these models to the LIGO/Virgo data from the O1 and O2 observing runs. We found that an initial BH mass spectrum $\propto M^{-2.35}$ is favored by the data, together with a maximum BH mass $M_{\max} \sim 50 M_{\odot}$. This is consistent with the theoretical upper limit for stellar BH masses, which is set by the occurrence of pair instability (Woosley 2017; Marchant et al. 2018).

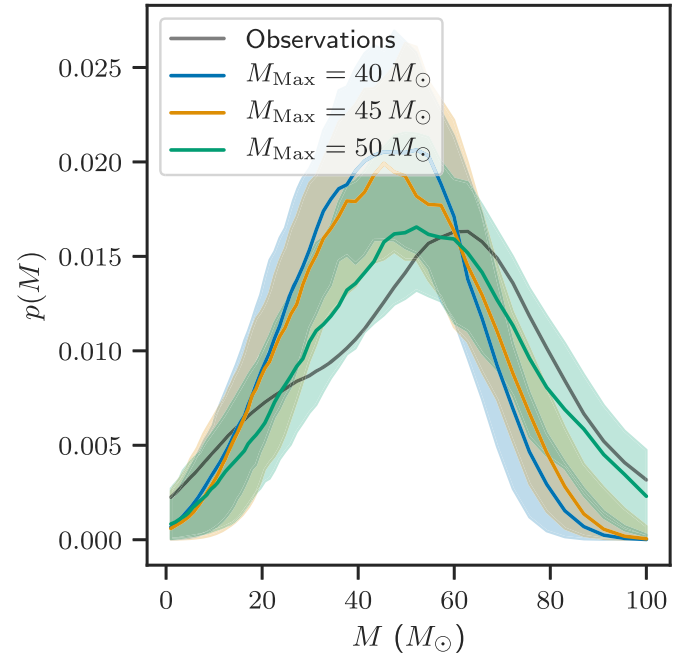


Figure 5. Comparison between the model prediction for the distribution of observed total mass after 10 observations for models at the indicated values of M_{\max} (with $\alpha = 2.35$) and the LIGO/Virgo observations (black line). The predictions from the models incorporate our estimate of the LIGO/Virgo selection function (Abbott et al. 2016c) and also estimate the observational uncertainties for each synthetic detection by matching to the LIGO/Virgo detection with the nearest median total mass. The solid line shows the median over 100 realizations of 10 simulated BBH detections from each model and the bands show the 1σ (68% credible) interval in the total mass distribution. None of the models fully reproduce the precise shape of the observed total mass distribution, but the observations remain within the 1σ uncertainty band for the model with $M_{\max} = 50 M_{\odot}$ throughout the entire mass range.

A slope $\propto M^{-2.35}$ reflects the initial mass function of massive stars, which is expected at the low metallicities required to form very massive BH remnants (i.e., Spera et al. 2015). Consequently, our work shows that dynamically formed binaries from low-metallicity stars are reasonably compatible with the binary BH mass distribution from the O1 and O2 LIGO/Virgo runs.

As more data is expected to be gathered in the years to come, statistical comparisons with numerical simulations will allow to establish whether the dynamical formation channel is indeed dominant, and to reconstruct the mass spectrum of the initial BHs, thus shedding a new light on massive stars and their evolution.

We thank Johan Samsing for valuable comments on our manuscript. R.P. acknowledges support from the NSF under grant AST-1616157. The Center for Computational Astrophysics at the Flatiron Institute is supported by the Simons Foundation.

ORCID iDs

Rosalba Perna  <https://orcid.org/0000-0002-3635-5677>

Will M. Farr  <https://orcid.org/0000-0003-1540-8562>

Matteo Cantiello  <https://orcid.org/0000-0002-8171-8596>

References

- Abbott, B. P., Abbott, R., Abbott, T. D., et al. 2016a, *ApJL*, **818**, L22
- Abbott, B. P., Abbott, R., Abbott, T. D., et al. 2016b, *PhRvL*, **116**, 061102
- Abbott, B. P., Abbott, R., Abbott, T. D., et al. 2016c, *ApJS*, **227**, 14
- Antonini, F., Chatterjee, S., Rodriguez, C. L., et al. 2016, *ApJ*, **816**, 65
- Antonini, F., Gieles, M., & Gualandris, A. 2019, *MNRAS*, **486**, 5008
- Banerjee, S. 2018, *MNRAS*, **473**, 909
- Belczynski, K., Holz, D. E., Bulik, T., & O’Shaughnessy, R. 2016, *Natur*, **534**, 512
- Chatterjee, S., Rodriguez, C. L., & Rasio, F. A. 2017, *ApJ*, **834**, 68
- Demorest, P. B., Pennucci, T., Ransom, S. M., Roberts, M. S. E., & Hessels, J. W. T. 2010, *Natur*, **467**, 1081
- Di Carlo, U. N., Giacobbo, N., Mapelli, M., et al. 2019, arXiv:1901.00863
- Dominik, M., Belczynski, K., Fryer, C., et al. 2013, *ApJ*, **779**, 72
- Farr, W. M. 2019, *RNAAS*, **3**, 66
- Farr, W. M., Stevenson, S., Miller, M. C., et al. 2017, *Natur*, **548**, 426
- Fishbach, M., Holz, D. E., & Farr, W. M. 2018, *ApJL*, **863**, L41
- Fragione, G., Grishin, E., Leigh, N. W. C., Perets, H. B., & Perna, R. 2018, arXiv:1811.10627
- Fragione, G., & Kocsis, B. 2018, *PhRvL*, **121**, 161103
- Generozov, A., Stone, N. C., Metzger, B. D., & Ostriker, J. P. 2018, *MNRAS*, **478**, 4030
- Harris, W. E. 1996, *AJ*, **112**, 1487
- Kalogera, V. 2000, *ApJ*, **541**, 319
- Leigh, N. W. C., Lützgendorf, N., Geller, A. M., et al. 2014, *MNRAS*, **444**, 29
- Madau, P., & Dickinson, M. 2014, *ARA&A*, **52**, 415
- Mandel, I., & de Mink, S. E. 2016, *MNRAS*, **458**, 2634
- Mandel, I., Farr, W. M., & Gair, J. R. 2019, *MNRAS*, **486**, 1086
- Mapelli, M., Zampieri, L., Ripamonti, E., & Bressan, A. 2013, *MNRAS*, **429**, 2298
- Marchant, P., Langer, N., Podsiadlowski, P., Tauris, T. M., & Moriya, T. J. 2016, *A&A*, **588**, A50
- Marchant, P., Renzo, M., Farmer, R., et al. 2018, arXiv:1810.13412
- Mikkola, S., & Merritt, D. 2008, *AJ*, **135**, 2398
- Miller, M. C., & Lauburg, V. M. 2009, *ApJ*, **692**, 917
- O’Leary, R. M., Rasio, F. A., Fregeau, J. M., Ivanova, N., & O’Shaughnessy, R. 2006, *ApJ*, **637**, 937
- Peters, P. C. 1964, *PhRv*, **136**, 1224
- Podsiadlowski, P., Rappaport, S., & Han, Z. 2003, *MNRAS*, **341**, 385
- Portegies Zwart, S. F., & McMillan, S. L. W. 2000, *ApJL*, **528**, L17
- Rodriguez, C. L., Amaro-Seoane, P., Chatterjee, S., & Rasio, F. A. 2018, *PhRvL*, **120**, 151101
- Rodriguez, C. L., Haster, C.-J., Chatterjee, S., Kalogera, V., & Rasio, F. A. 2016, *ApJL*, **824**, L8
- Rodriguez, C. L., & Loeb, A. 2018, *ApJL*, **866**, L5
- Roulet, J., & Zaldarriaga, M. 2019, *MNRAS*, **484**, 4216
- Ryu, T., Tanaka, T. L., & Perna, R. 2016, *MNRAS*, **456**, 223
- Salpeter, E. E. 1955, *ApJ*, **121**, 161
- Samsing, J. 2018, *PhRvD*, **97**, 103014
- Samsing, J., & D’Orazio, D. J. 2018, *MNRAS*, **481**, 5445
- Sigurdsson, S., & Hernquist, L. 1993, *Natur*, **364**, 423
- Spera, M., Mapelli, M., & Bressan, A. 2015, *MNRAS*, **451**, 4086
- The LIGO Scientific Collaboration, & the Virgo Collaboration 2018, arXiv:1811.12907
- The LIGO Scientific Collaboration, the Virgo Collaboration, Abbott, B. P., et al. 2018, arXiv:1811.12940
- Wang, Y.-H., Leigh, N., Sesana, A., & Perna, R. 2019, *MNRAS*, **482**, 3206
- Wiktorowicz, G., Belczynski, K., & Maccarone, T. 2014, in Conf. Proc. Binary Systems, their Evolution and Environments, **37**
- Woolley, S. E. 2017, *ApJ*, **836**, 244
- Ye, C. S., Kremer, K., Chatterjee, S., Rodriguez, C. L., & Rasio, F. A. 2019, arXiv:1902.05963
- Zhou, S., Evans, N. J., II, Wang, Y., Peng, R., & Lo, K. Y. 1994, *ApJ*, **433**, 131
- Ziosi, B. M., Mapelli, M., Branchesi, M., & Tormen, G. 2014, *MNRAS*, **441**, 3703